Measurement of NO_2^- penetration concentration in surface microdischarge treated model tissue, based on image processing technology

Bingkai Wang, Yuqi Wang, Zilan Xiong*

State Key Laboratory of Advanced Electromagnetic Engineering and Technology

Huazhong University of Science and Technology,

Wuhan, China

zilanxiong@hust.edu.cn

***Abstract*—Plasma has a wide range of applications in the medical field. The reactive oxygen species and reactive nitrogen species generated by plasma play a major role during the plasma treatment. However, the measurement of penetration concentration of reactive species into tissues has always been a major problem in the application of plasma medicine. In this paper, based on the digital image processing technology, we realized the measurement of NO_2^- penetration concentration inside model tissues by SMD treatment. Firstly, based on the specific color reaction of Griess and NO_2^-, the multivariate linear relationship between image color and standard concentration was established. Then, the model tissues were treated by SMD under different time and treating distance. Finally, the concentration of each point in each layer of the model tissue under SMD treatment was measured and calculated. It is found that the NO_2^- concentration distribution in the central part of each layer was uniform under SMD treatment, and the concentration gradually decreased with the penetration depth. This study offers a fast and smart diagnostic method for reactive species amount into tissue and provide data for clinic as well as numerical modeling investigation.**

Keywords—model tissue, SMD, NO_2^- concentration, image processing

I. INTRODUCTION

In recent years, cold atmospheric plasma has been widely used in the biomedical field [1]. The reaction mechanism of plasma and tissue is still under investigation by groups worldwide, but it is widely accepted that the reactive nitrogen species (RNS) and reactive oxygen species (ROS) play an important role in the treatment process[2], including long-lived species such as NO_2^-, NO_3^-,H_2O_2, O_3, and short-lived species such as O and OH. During the plasma treatment of biological tissues, the complex physical and chemical composition leads to the penetration of species with tissues, which makes it difficult to achieve accurate diagnosis of species that penetrate into the tissue. This has become one of the key problems in explaining the relationship between RONS dose and treatment effect [3]. To facilitate studies, gelatin [4] or agarose [5] models are usually used instead of real human tissues. Gelatin models use animal tissue extracts, which have many similarities with human tissues in composition and structure.

This work was supported by the National Natural Science Foundation of China, Grant Number: 51907076.

At present, the diagnosis of RONS penetration amount is mainly qualitative approach. Color-forming reactions such as KI-Starch and Griess can indicate the distribution and relative amount of RONS, and the depth of color can be used to reflect the amount of RONS penetration[6]–[10]. The quantitative diagnostic approach for RONS penetration amount is mainly the measurement of penetration depth[11], [12] or transformed into indirect liquid phase measurements [13]–[15].

None of the existing diagnostic schemes are capable of quantitative diagnosis for the spatial distribution of RONS concentration in plasma-treated tissue. In our previous study, a low-cost solution for accurate diagnosis of liquid-phase NO_2^- was proposed based on digital image processing technology [16]. In this investigation, we further developed this method to the quantitative diagnosis of NO_2^- concentration in model tissues. In order to make a simulated human tissue model with better biosimilarity, a gelatin-polysaccharide model was used in this study. Based on digital image processing technology, the correspondence between the color and standard concentration was obtained. A SMD device was used to produce the reactive species. The samples were treated with different time and treating distance. The spatial concentration distribution of each layer of the plasma-treated model tissues could be measured after image processing and data analysis.

II. MATERIALS AND METHODS

A. Reaction Principle

During plasma treatment of human tissues, NO_2^- (one of the main RNS species in aqueous phase) will be produced when the gas phase products containing RNS contacts with the tissue. The NO_2^- and Griess can have a specific chromogenic reaction with a ratio of 1:1 [17]. As shown in Fig.1, NO_2^- first reacts with sulfonamide in an acidic environment to form a diazo compound, and later couples with N-naphthyl-ethylenediamine to form a stable magenta color azo complex. The degree of color varies with different NO_2^- concentrations, so the quantitative relationship between concentration and color can be obtained by exploring the color characteristics under the reaction of standard concentration NO_2^- with sufficient amount of Griess.

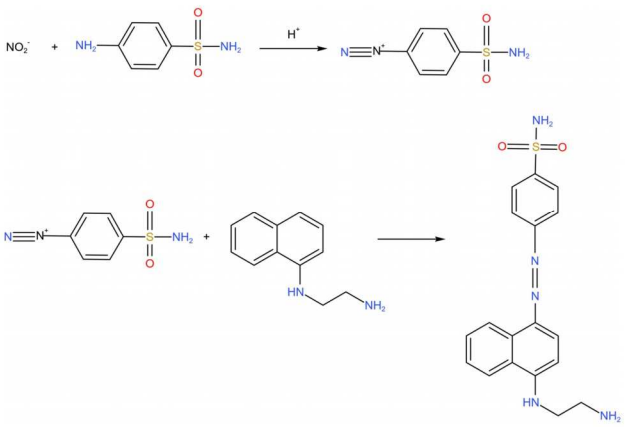

Fig.1. Reaction of NO_2^- and Griess.

B. Sample Preparation

As shown in Fig.2, the sample preparation is divided into four parts:

First, 15% gelatin (Sigma–Aldrich) and 2% starch (Sinopharm) were prepared as model tissue, mixed with Griess (0.68% sulfonamide, Sinopharm; 0.21% N-naphthyl-ethylenediamine, Sinopharm; 1.39% citric acid, Sinopharm; with a theoretical detectable NO_2^- concentration of 4000μM). Drop the standard concentration (0, 50, 100, 150, 200, 400, 600, 800, 1000, 1500, 2000, 3000μM) of $NaNO_2$ (Sinopharm) into the model tissue and stir until the color was uniform. And then the model tissue was poured into a 22mm petri dish to solidify.

Second, the model tissue was frozen to −20 °C by a freezing microtome (Leica, CM 1950) for 20 min, and then sliced at 100μm for taking pictures by camera (NIKON).

Third, five images were acquired at each standard concentration, which can effectively reduce the error.

Fourth, the images were moved to computer for image processing (OpenCV-Python) and data analysis.

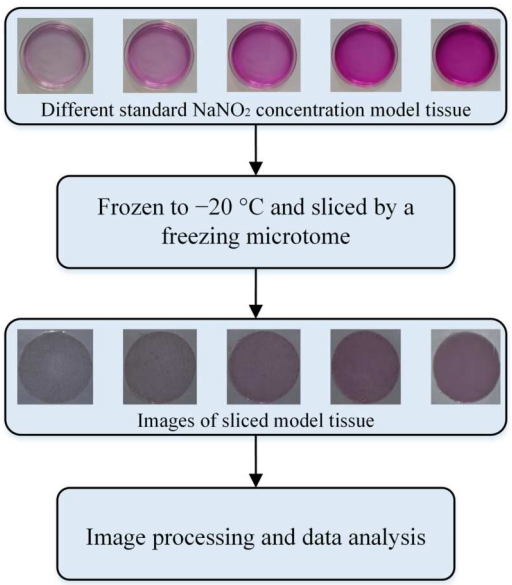

Fig.2. The general procedure of sample preparation.

C. Image Processing and Data Analysis

After image shooting, the contours of the model tissue was extracted. Then the circle fitting to the contour classes was conducted, and the circular contours was visualized. Finally, the average color of the slice area could be obtained by digital image processing. With a tested segmented linear fitting method based on H value, with the RGB values as the fitted independent variables, and NO_2^- concentration C (μM) as the dependent variable, the concentration of each pixel point in the sliced area regardless of the shape size could be calculated.

D. Experimental setup and treatment

Fig.3 shows the schematic diagram of the SMD experimental setup. The SMD device was divided into three parts: high voltage electrode, insulating medium and ground electrode. Here, a copper cylinder with a diameter of 30mm was used as the high voltage electrode and a stainless-steel mesh was used as the ground electrode, and the insulating medium was placed between the high voltage and the ground electrode using a 1mm thick ceramic plate. A sinusoidal voltage with a peak-to-peak value of 12.2 kV and a frequency of 8 kHz was used for the AC power supply (CTP-2000K; Corona Lab). The applied voltage was monitored using a voltage probe (Tektronix; P6015A) and the circuit current was measured using a current probe (Pearson 6585). A 10nF capacitor was connected in series between the mesh and the ground. The voltage across the capacitor was measured using a differential probe (Tektronix P5200A). The waveforms were recorded by an oscilloscope (Tektronix DPO2024B). A Fourier Transform Infrared Spectroscopy (VERTEX 70; Bruker) was used as an in situ diagnostics of the gas phase products produced by the SMD.

The model tissue was put inside a petri dish with 22 mm in diameter and 10 mm in height, and the model tissue filled the petri dish exactly. During treatment, the petri dish was placed directly below the SMD electrode inside a closed cylindrical cavity. The samples were divided into different groups by treated for 20, 40 and 60 s and at distance of 15, 25 and 35 mm, respectively.

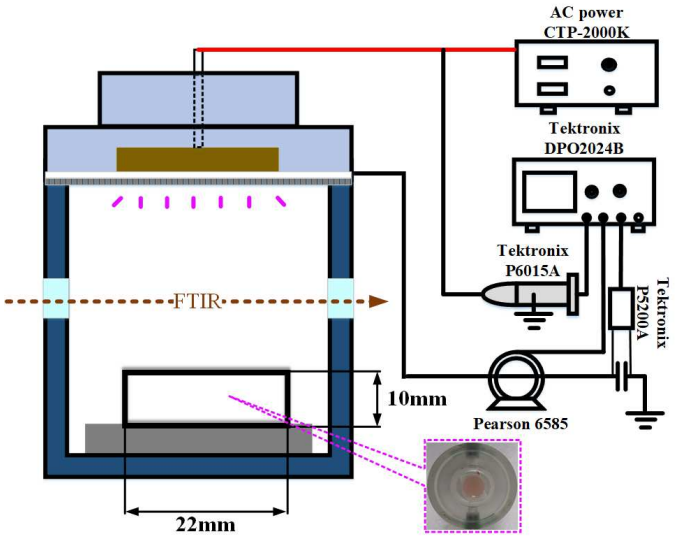

Fig.3. Schematic diagram of the SMD experimental setup.

III. Results and Discussion

A. Voltage and current during discharging

The voltage and current waveforms are shown in Fig.4. The voltage is a standard sinusoidal wave with a peak-to-peak value of 12.2 kV and the frequency is fixed at 8kHz. The current fluctuates greatly near the junction of positive and negative voltage values, especially from negative to positive. The discharge power was measured using the Lissajous method and was fixed at 7W.

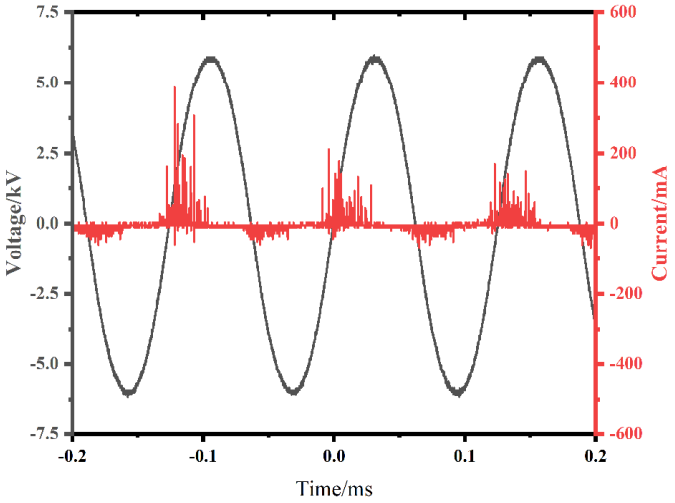

Fig.4. U–I waveform of the SMD.

B. FTIR of the gas phase products

As the discharge progressed, a series of gas-phase products were produced and diffused throughout the chamber. These gas-phase products biochemically reacted with the surface of the model tissue, resulting in liquid-phase products that penetrated into the tissue. To explore the composition of the gas-phase products, we measured the compositional changes at 20s, 40s, and 60s at 7W power supply using FTIR, as shown in Figure 5. The gas phase products are mainly a series of nitrogen oxides species including NO, NO_2, N_2O, N_2O_5, and the accumulation increases with time. The liquid-phase reaction of NO_x with the surface of the model tissue results in the penetration of NO_2^- into the tissue.

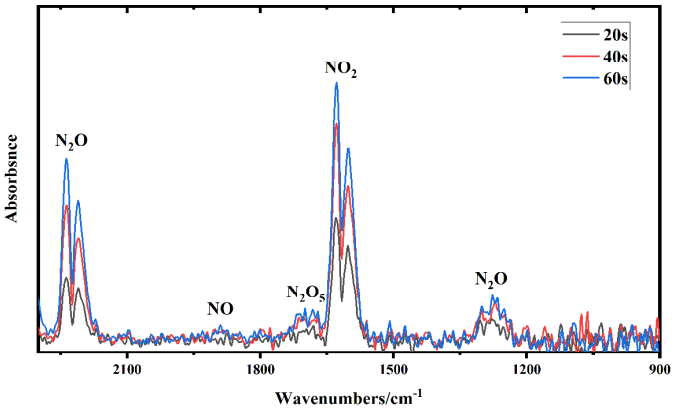

Fig.5. FTIR spectrum of gas phase products at 20s, 40s, 60s.

C. Surface Distribution of Treated Model Tissue

The surface distribution of treated model tissue is shown in Fig.6. It could be found that the color distribution on the surface of the model tissue after SMD treatment was uniform. Under the same distance, as the treatment time increased, the surface color gradually became darker; under the same treatment time, as the distance increased, the surface color gradually became lighter. The bare eyes can only tell the color nuance between different samples. According to our previous research results, color distribution and depth were directly related to NO_2^- concentration and amount. The concentration distribution of each layer was then obtained by image processing technology.

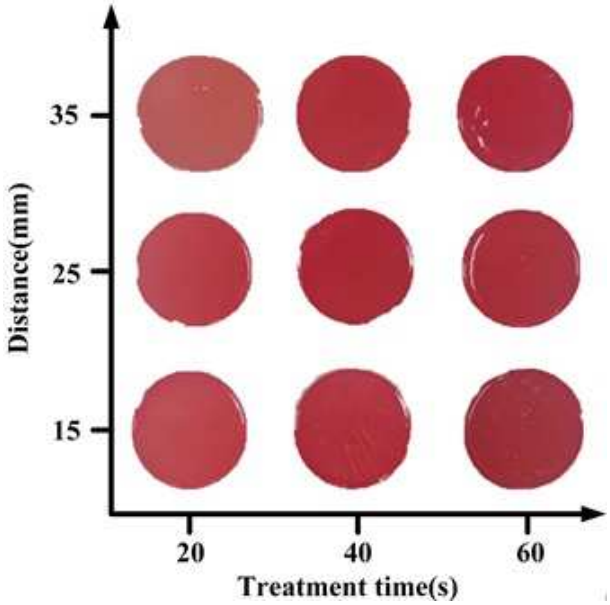

Fig.6. Effects of treatment time and distance on surface distribution of treated model tissue.

D. Cross-sectional Concentration Distribution

After obtaining the image of the slice region, the concentration value of each pixel point was obtained. As shown in Fig.7, multiple concentration distribution maps sampled from the chromogenic layer depicted the NO_2^- spatial distribution penetrated in the model tissue under SMD treatment. The concentration distribution in the central part of each slice was approximately uniform, but a higher concentration distribution appears at the edges. This was due to the boundary of the container during the diffusion process, resulting in the accumulation of NO_2^-. If the model tissue was large enough, uniform infiltration could be achieved.

For the spatial distribution, it could be seen in Fig.7 that the concentration distribution of each layer gradually became lighter in color as the penetration depth deepened. The average concentration in the section area of each layer section was calculated and the trend of the average concentration of each layer section with the layer number was plotted, as shown in Fig.8. It could be found that the average concentration of each layer tended to decrease gradually at the same treatment time with different distance. At the same time, under the same treatment time, the smaller the treatment distance, the higher the overall osmotic concentration.

Most of the existing reactive species (in tissue) measurement methods cannot directly quantitatively measure the concentration. Although UV-Vis absorbance can measure reactive species in tissues, due to the limitation of aperture size, the spatial distribution of reactive species cannot be accurately measured, and additional optical paths and control platforms will increase the cost and difficulty. The proposed method is fast and smart, but there is also the problem of light interference in image processing, which can be improved by fixing the light source and measuring multiple times. Meanwhile, since the auxiliary operation of the slicer is used, which brings inconvenience to the practical application, the three-dimensional distribution reconstruction can be realized by combining the two-dimensional plane image and the penetration depth in the future.

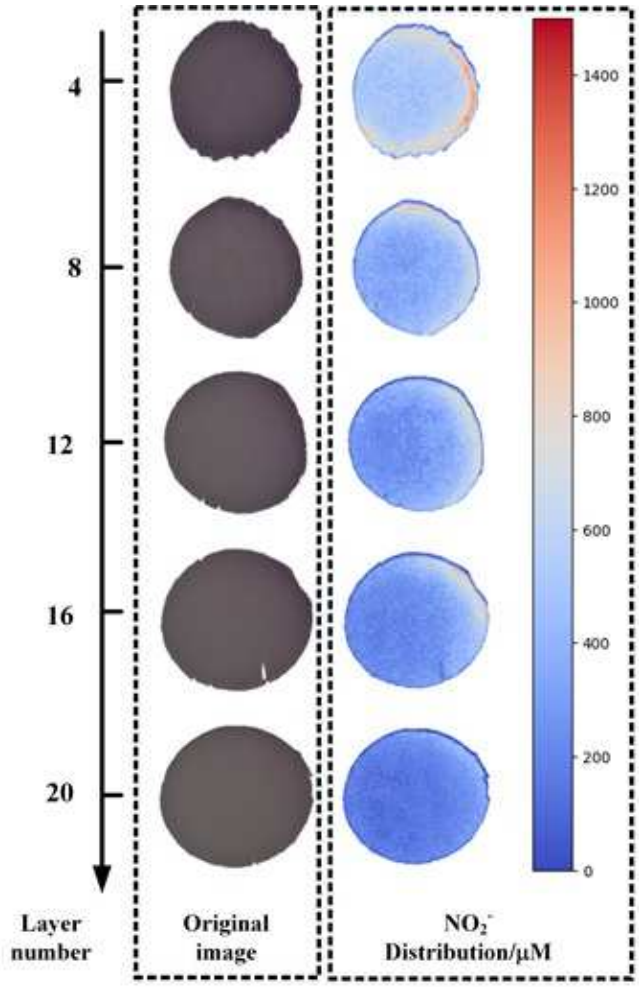

Fig.7. The NO_2^- distribution of layer 4,8,12,16,20 at 20s with treatment distance at 35mm.

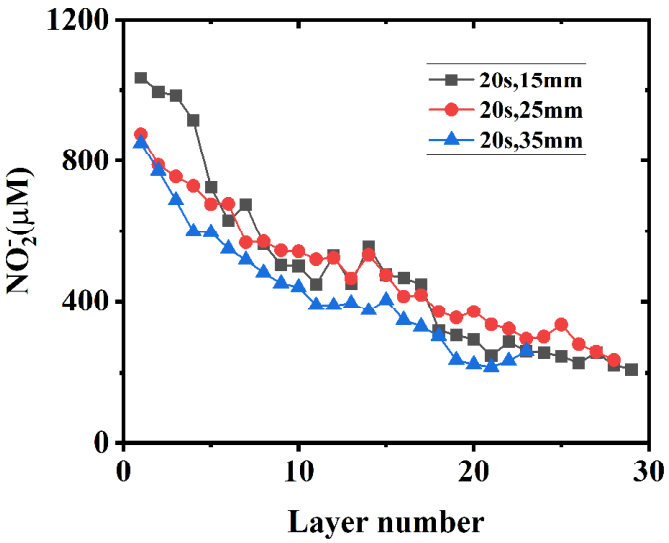

Fig.8. Average concentration with layer number at 20s with treatment distance at 15mm, 25mm, 35mm, respectively.

IV. Conclusion

In this paper, we established a linear relationship between NO_2^- concentration and RGB pixel values using digital image processing technology and the chromogenic reaction of Griess with standard concentration of NO_2^- with H value as the segmentation condition, and achieved accurate point-to-point concentration measurement in cross-section.

For the spatial distribution characteristics at 15, 25 and 35mm distance of SMD treatment for 20, 40 and 60 s, the spatial distribution of the penetration concentration of each layer of the slices was almost uniform, and the average concentration of each layer gradually decreased as the permeation depth increased. Through this method, we could realize the measurements of spatial and temporal distribution of reactive species inside the treated tissue, and offers a new method for fast and smart measurement in plasma medicine.

References

[1] G. Lloyd, G. Friedman, S. Jafri, G. Schultz, A. Fridman, and K. Harding, "Gas plasma: Medical uses and developments in wound care," *Plasma Process. Polym.*, vol. 7, no. 3–4, pp. 194–211, 2010, doi: 10.1002/ppap.200900097.

[2] D. B. Graves, "The emerging role of reactive oxygen and nitrogen species in redox biology and some implications for plasma applications to medicine and biology," *J. Phys. D. Appl. Phys.*, vol. 45, no. 26, 2012, doi: 10.1088/0022-3727/45/26/263001.

[3] E. J. Szili, S. H. Hong, J. S. Oh, N. Gaur, and R. D. Short, "Tracking the Penetration of Plasma Reactive Species in Tissue Models," *Trends Biotechnol.*, vol. 36, no. 6, pp. 594–602, 2018, doi: 10.1016/j.tibtech.2017.07.012.

[4] D. Dobrynin, G. Fridman, G. Friedman, and A. Fridman, “Deep penetration into tissues of reactive oxygen species generated in floating-electrode dielectric barrier discharge (FE-DBD): An in vitro agarose gel model mimicking an open wound,” *Plasma Med.*, vol. 2, no. 1–3, pp. 71–84, 2012, doi: 10.1615/PlasmaMed.2013006218.

[5] J. S. Oh *et al.*, “How to assess the plasma delivery of RONS into tissue fluid and tissue,” *J. Phys. D. Appl. Phys.*, vol. 49, no. 30, 2016, doi: 10.1088/0022-3727/49/30/304005.

[6] T. Kawasaki, W. Eto, M. Hamada, Y. Wakabayashi, Y. Abe, and K. Kihara, “Detection of reactive oxygen species supplied into the water bottom by atmospheric nonthermal plasma jet using iodine-starch reaction,” *Jpn. J. Appl. Phys.*, vol. 54, no. 8, 2015, doi: 10.7567/JJAP.54.086201.

[7] T. Kawasaki *et al.*, “Transportation of reactive oxygen species in a tissue phantom after plasma irradiation,” *Jpn. J. Appl. Phys.*, vol. 57, no. 1, 2018, doi: 10.7567/JJAP.57.01AG01.

[8] T. Kawasaki, F. Mitsugi, K. Koga, and M. Shiratani, “Local supply of reactive oxygen species into a tissue model by atmospheric-pressure plasma-jet exposure,” *J. Appl. Phys.*, vol. 125, no. 21, 2019, doi: 10.1063/1.5091740.

[9] A. Nakajima *et al.*, “Effects of gas flow on oxidation reaction in liquid induced by He/O2 plasma-jet irradiation,” *J. Appl. Phys.*, vol. 118, no. 4, 2015, doi: 10.1063/1.4927217.

[10] T. Kawasaki *et al.*, “Visualization of the distribution of oxidizing substances in an atmospheric pressure plasma jet,” *IEEE Trans. Plasma Sci.*, vol. 42, no. 10, pp. 2482–2483, 2014, doi: 10.1109/TPS.2014.2325038.

[11] T. He *et al.*, “Transportation of ROS in model tissues treated by an Ar + O2 plasma jet,” *J. Phys. D. Appl. Phys.*, vol. 52, no. 4, 2019, doi: 10.1088/1361-6463/aaed6f.

[12] D. Liu *et al.*, “Spatial-temporal distributions of ROS in model tissues treated by a He+O2 plasma jet,” *Plasma Process. Polym.*, vol. 15, no. 10, pp. 1–8, 2018, doi: 10.1002/ppap.201800057.

[13] L. Nie, Y. Yang, J. Duan, F. Sun, X. Lu, and G. He, “Effect of tissue thickness and liquid composition on the penetration of long-lifetime reactive oxygen and nitrogen species (RONS) generated by a plasma jet,” *J. Phys. D. Appl. Phys.*, vol. 51, no. 34, 2018, doi: 10.1088/1361-6463/aad427.

[14] J. Duan, L. Gan, L. Nie, F. Sun, X. Lu, and G. He, “On the penetration of reactive oxygen and nitrogen species generated by a plasma jet into and through mice skin with/without stratum corneum,” *Phys. Plasmas*, vol. 26, no. 4, 2019, doi: 10.1063/1.5082160.

[15] J. Duan, X. Lu, and G. He, “On the penetration depth of reactive oxygen and nitrogen species generated by a plasma jet through real biological tissue,” *Phys. Plasmas*, vol. 24, no. 7, 2017, doi: 10.1063/1.4990554.

[16] Z. Zou, R. Han, C. Lu, and Z. Xiong, “Detection of long-lived species in plasma-activated water, based on digital colorimetry,” *Plasma Process. Polym.*, vol. 18, no. 1, pp. 1–12, 2021, doi: 10.1002/ppap.202000139.

[17] J. Sun, X. Zhang, M. Broderick, H. Fein, W. P. Instruments, and S. International, “JEI SON 2003sensors-03-00276,” *Sensors*, vol. 3, pp. 276–284, 2003, [Online]. Available: http://www.mdpi.net/sensors.